T.1 : Soft x-ray laser at 46.9 nm from argon plasma

S. Barnwal, S. Nigam* and Y.B.S.R. Prasad
*Laser Plasma Division / *Laser Electronics Support Division*
E.mail : sbarnwal@rrcat.gov.in

1. Introduction : Lasing action in the short wavelength region of the spectrum has been an area of great interest right from the invention of laser. Sustained efforts have been put world over to extend the wavelength of lasers towards x-ray region as x-ray lasers have many applications in wide areas of science and technology. In fact, several new applications may come up in future, if such coherent x-ray sources become available in the laboratory. Various groups have been successful in their efforts of demonstrating x-ray laser using various techniques which include x-ray free-electron lasers (FEL), plasma based x-ray lasers, and coherent x-ray radiation through high-order harmonic generation. Plasma based x-ray lasers may again be classified into two categories, one based on laser produced plasma and the other based on the plasma created by fast capillary discharges. All these approaches are complimentary to each other in their advantages and limitations. The x-ray laser from laser produced plasma has the advantage of short pulse duration but suffers from smaller gain volume resulting in lower flux and no tunability, although, they can be generated at different wavelengths by changing the gain medium. Coherent x-ray radiation from high order harmonic generation is partially tunable and offer high brightness, but has a low conversion efficiency. X-ray FEL is the most successful coherent x-ray source till date, in terms of high brightness, broad tunability, and high average power. However, these are big facilities which are very expensive to construct and cannot be used as compact sources in laboratory. On the other hand, x-ray laser based on fast electric discharges in a gas filled capillary provides a very promising alternative to the aforesaid schemes of making x-ray laser. This scheme delivers higher photon flux in the lasing wavelength than any laser driven scheme. Also, soft x-ray laser based on capillary discharge scheme offers a very compact size compared to big facilities such as FELs or high power laser based x-ray lasers.

Considering these facts, the efforts were started more than two decades ago to build x-ray laser using capillary discharge scheme. The first experimental demonstration of soft x-ray lasing at 46.9 nm from argon z-pinch plasma was by Rocca *et al* [1]. The coherent amplification at 46.9 nm wavelength is from $3s\ ^1P_1$ -$3p\ ^1S_0$ transition in Ne-like Ar (Ar^{8+}) ions, which is realized through electron collisional excitation. Subsequently, table-top soft x-ray laser in the saturated regime has also been demonstrated [2,3]. Ben-Kish *et al* [4] showed the important role of pre-pulse in this lasing scheme [5]. Later on, groups from Japan [6-9], Italy [10-13], Malaysia [14,15], China [16-19] and Czech Republic [20] have also demonstrated lasing at 46.9 nm using the capillary discharge scheme.

This activity was started few years back at RRCAT as a joint project of Laser Plasma Division and Laser Electronics Support Division, with an aim to build first soft x-ray laser in India. With continuous directed efforts, soft x-ray lasing at 46.9 nm in argon plasma was successfully demonstrated in our laboratory. This is the first soft x-ray laser in our country. It has been subsequently characterized for its various parameters e.g. pulse duration, divergence, pulse energy, and spatial coherence.

In the subsequent sections of this article, we will give some details about the population inversion mechanism and the fast capillary discharge scheme. This will be followed by details of the different experiments done in our laboratory towards building as well as characterization of this soft x-ray laser.

2. Schemes of achieving population inversion in plasma: The major schemes of achieving population inversion in plasma are via: a) collisional excitation scheme and b) recombination scheme. There are some other schemes also like resonant photo excitation, which are not very successful.

2.1 Collisional excitation : In this scheme, a closed shell configuration of ion is used, as ions having closed shell configuration, such as He-like (2), Ne-like (10) and Ni-like (28), have a much higher fractional abundance compared to their neighbours. For Ne-like ions, the ground state configuration is $1s^2\ 2s^2\ 2p^6$ (ground state: $^1S_0$). The first excited state is $2p^5\ 3s$: $^1P_1$ and the next higher state is $2p^5\ 3p$, which has S and D states. Collisional excitation from ground state to both these excited states is allowed. As a result, both these levels get populated by collisional excitation from the ground state. Radiative transition between 3s level to 2p level is allowed , but not from 3p level. Hence, the population in 3s level quickly decays to ground state but that of 3p state cannot. One thus gets population inversion between these two excited levels 3p and 3s. Radiative transition between these levels is an allowed transition (lasing transition). Using these scheme, first x-ray laser was successfully demonstrated in 1985 [21]. The lasing was in Ne-like Se^{24+} ions at 20.63 nm and 20.96 nm. Subsequently, lasing action has been demonstrated in Ne-like strontium (Z=38), molybdenum (Z=42), silver (Z=47) etc

2.2 Collisional recombination : This scheme is based on three body recombination of closed shell configuration ions to single outer shell electron (e.g. fully ionized to H-like, He-like to Li-like, Ne-like to Na-like etc.). When ions undergo three body recombination, it captures a free electron in a level which is within energy of the order of kT_e from the ionization limit. The excess energy ($\sim kT_e$) is given to a third particle (another free electron). If kT_e is less than few tens of eV, the recombination takes place in high n levels. As the electron cascades down, one gets population inversion (usually between n = 3 to n=2 levels, i.e. the Balmer-α transition). The recombination rate is given as $R_{3br} \sim n^4 n_e^2 T_e^{-4.5}$, where n is the principal quantum number, n_e is the electron density in plasma, and T_e is the plasma temperature. This expression clearly indicates that this process is dominant for cold and dense plasmas. It requires faster recombination to get inversion. Using this scheme, lasing has been observed in H-like carbon, fluorine, sodium etc. Lasing on Balmer-α line of carbon at 18.2 nm was demonstrated in 1985 by Suckewer *et al* [22] at the same time as the collisionally pumped laser. Subsequently, lasing has been observed in Li-like ions in plasma of aluminum (Z=13), titanium (Z=22) etc.

3. Capillary discharge scheme for soft x-ray lasing : In this scheme, a fast rising (few tens of ns), large amplitude (~ few tens of kA) current pulse ($dI/dt > 10^{11}$ A/s) is passed through a plasma column in a capillary as shown in Fig.1. Building a pulsed power system delivering such fast as well as high current is by itself a challenging task. Usually, in order to generate current pulse with a fast rise time, a waterline capacitor is charged up to few hundreds of kilovolts using a Marx bank and then discharged through the gas column using a fast switch (usually a pressurized spark gap). It is experimentally seen that in order to get reliable lasing action it is essential to pass the main discharge current through a pre-ionized gas rather than neutral gas. It is found that this reduces the plasma instabilities leading to reliable lasing action. The pre-ionization is achieved by passing a 10-50 A current pulse a few μs before the main current. Since the pre-formed plasma has very high conductivity, the main current flows through a thin outer layer (within skin depth) of the plasma column. The high discharge current generates a large magnetic field in the azimuthal direction and the resulting radial JxB force compresses the plasma column radially inwards i.e. from the wall towards the axis, as shown in the Fig. T.1.1. A high value of 'dI/dt' helps in fast detachment of this plasma column from the wall of the capillary, thereby minimizing the impurities from the wall in the plasma. During the radial compression (pinching) of the plasma column, the temperature and ionization of the plasma column significantly increases due to

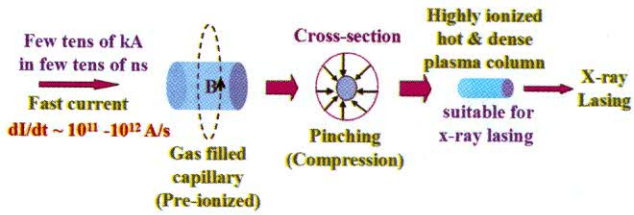

Fig. T.1.1: Pinching action due to the magnetic field

enhanced collisions between the electrons and the ions. As a result, a highly ionized, hot, dense plasma column is formed (Z–pinch). As the compression progresses, the density and the temperature of the plasma increases till the kinetic pressure ($n_e kT$) acting in the radially outward direction becomes equal to the Lorentz force acting in the radially inward direction. This is known as the Bennett's equilibrium condition [23]. The pre-ionization helps in achieving a high axial uniformity throughout the plasma column having a large length to diameter aspect ratio of the order of 1000:1. Optimization of different experimental parameters is required to achieve a high abundance of Ne-like argon ions (the lasing species) in the plasma and also for achieving population inversion between the appropriate lasing levels populated through collisional excitation by the plasma electrons.

The hot, dense plasma column lasts for a very short duration, after which it expands outwardly towards the capillary wall. This occurs due to the radially outward kinetic pressure as the radially compressing magnetic force due to the Lorentz force starts loosing its strength once the current pulse starts decreasing. The efficient pinching of plasma column depends on various parameters like pre-plasma conditions, discharge current, gas pressure in the capillary etc. In order to have a abundant Ne-like Ar^{8+} species, simulations predict an optimum electron density of $\sim 10^{18\text{-}19}$ cm^{-3}, and temperatures in the range of 60-80 eV, in addition to a suitable electron density profile and a small transverse dimension of the plasma column [24,25].

Based on this scheme, very compact table top (1 m × 0.4 m) saturated 46.9 nm lasers of size has been developed by Rocca *et al.* [26-27]. This laser was successfully used to perform high resolution soft x-ray laser interferometry and shadowgraphy of plasmas. Recently, another capillary discharge soft x-ray laser was operated at a repetition rate of 7 Hz to produce an average output pulse energy of 135 μJ, corresponding to an average laser power of ~1 mW. The latest result includes the generation of laser pulses at an average energy of 0.88 mJ at a rep rate of 4 Hz in a highly saturated amplifier [28].

4. High voltage capillary discharge x-ray laser setup : After a brief review of the different capillary discharge based x-ray laser systems developed in other laboratories, we will now discuss about the developments and experiments conducted in our laboratory in this field. The discussion will also cover some aspects of the electrical design of the system which is very crucial for making this laser. A schematic diagram of the first version of our capillary discharge x-ray laser setup is shown in Fig. T.1.2 and a photograph of the new compact version is shown in Fig. T.1.3.

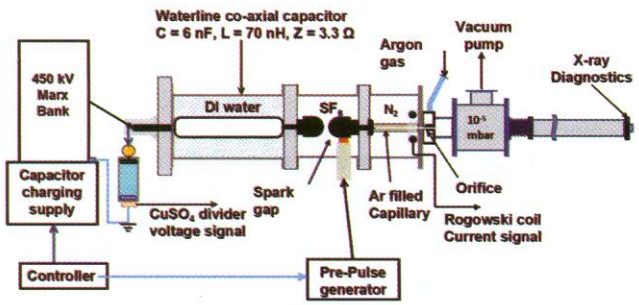

Fig. T.1.2: Schematic diagram of our capillary discharge x-ray laser setup (Version 1)

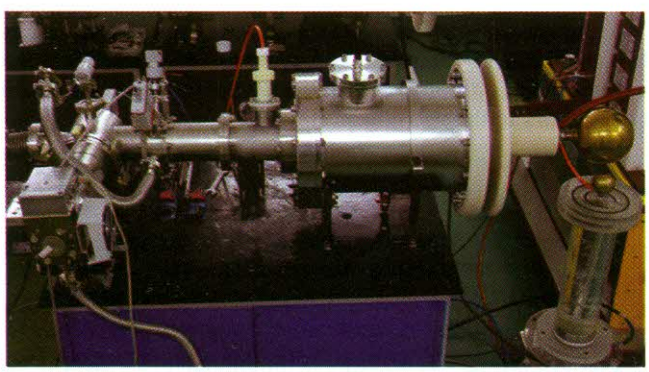

Fig. T.1.3: Photograph of the compact system (Version 2)

The requirement of fast discharge current (few tens of kA in few tens of ns) for soft x-ray lasing was fulfilled by an indigenously developed pulse power system. The system has a 450 kV, 10-stage Marx bank which was erected upto ~ 300 kV for the experiments. This Marx bank charges a pulse forming line in the form of a waterline coaxial capacitor (C = 6 nF, L = 70 nH and Z = 3.3 Ω) filled with de-ionized water. De-ionized water was used due to its low conductivity (< 2.0 μS) leading to low leakage current and high dielectric constant (80) leading to high breakdown strength. The waterline capacitor was connected in series to the ceramic capillary (length 15 cm and diameter 2.8 mm) through a fast switch in the form of a pressurized (with SF_6) spark gap. The other end of the capillary was grounded. Therefore, when the charged voltage on the capacitor crosses the breakdown voltage of the spark gap switch, the switch closes and a large current flows rapidly through the gas filled in the capillary. The breakdown voltage of the spark gap could be controlled by changing the electrode gap or by changing the SF_6 gas pressure. SF_6 gas was used in the spark gap due to its high breakdown strength and excellent arc-quenching property. The fast waterline capacitor and spark gap switch act in combination and help in providing fast current with rise-time of the order of few nanoseconds which otherwise would have duration in microseconds. An in-house developed pre-pulse generator was used to create pre-pulse (15-40 A) required for creating a pre-plasma in the capillary 5-10 μs before the main current pulse. A 1 mm orifice acts like the ground electrode for the capillary discharge allowing the x-ray coherent radiation to pass through it, in addition to helping in maintaining differential vacuum between the capillary side and the diagnostics side. The diagnostics section was evacuated with a turbo-molecular pump (< 10^{-4} mbar) to minimize the absorption of the soft x-ray laser signal. The argon gas (lasing medium) was continuously fed into capillary chamber through a small port near the capillary ground electrode using a fine gas dosing and regulating valve.

The main discharge current was monitored using a calibrated Rogowski coil placed around the ceramic capillary. The voltage at the Marx generator output stage was measured using a $CuSO_4$ voltage divider. The temporal profile of the plasma emission from the capillary was recorded using either a bi-planar vacuum diode or a quadrant diode developed in-house. The signals were recorded on an oscilloscope (1 GHz, 10 GS/s). Such pulsed power systems with high current electrical discharge pose large noise problems in the sensitive electronic circuits. During the discharge shot, significant electro-magnetic interference (EMI) is generated which interferes with the control systems, measuring instruments and diagnostic equipments. Hence, in order to minimize EMI, all the diagnostics and instruments were kept in an EMI shielded Faraday cage. Also, special double shielded cables were used to carry the signals from one place to the other.

The crucial part of this system is the fast discharge circuit, comprising of the coaxial water capacitor, the spark gap and the 150 mm long, 2.8 mm inner diameter ceramic capillary. The capillary is filled with argon gas and is pre-ionized so that it acts as a conductor for the main discharge current to pass through it. All these components are made in a co-axial geometry to reduce the inductance of the circuit. Simulations were carried out to understand the discharge behaviour of these components which helps us to get the electrical equivalent of the discharge circuit as shown in the Fig. T.1.4 to optimize different system parameters.

A brief discussion of the electrical equivalent of our system is as follows. The first section of the model is of the Marx generator having total capacity Cm=6 nF and charged

initially to the high voltage. The generator gives a pulsed output after switch U_m closes at the instant t=0. The experimentally determined Marx generator's series parameters : inductance Lm and resistance R_m, are 11 μH and 3 ohm respectively. Second part is the voltage divider (with a ratio of 2500:1, used to monitor the erected voltage) as a resistance R_d. This part is included in the simulation as it appears as a load to the Marx generator, in parallel with the fast capacitor.

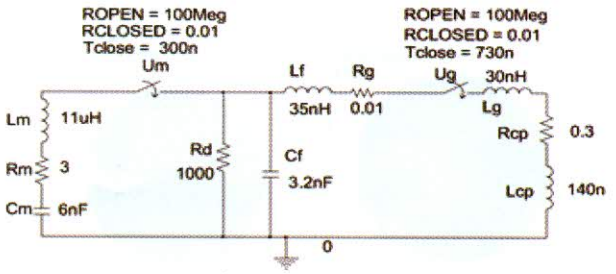

Fig. T.1.4: Electrical equivalent circuit diagram of the pulse discharge system.

The larger resistance of the divider is made from copper sulphate solution. The smaller one is made from twenty 10 ohm (2 W) resistances connected in parallel, resulting into 0.5 ohm. The geometry of the fast capacitor is like a coaxial line but frequencies involved in the system are not high enough to consider it as a distributed ladder or a cable in the model. Therefore, it is represented in our model as a lumped capacitor C_f. The spark gap section is modeled using a closing switch U_g along with series inductance Lg. The capillary section is modeled as resistance R_{cp} (~0.4 ohm) and series inductance L_{cp} of ~150 nH for ~140 mm long plasma column [29]. The fast capacitor gets charged from the Marx generator and its discharge into capillary takes place when the spark gap and the capillary break down (practically at same instant, since capillary is pre-ionized). Pulse rises at the Marx generator output when the switch U_m is closed at t=0. To get breakdown at the desired voltage of erection, the closing time of the U_g and the U_{cp} is shifted to the required value. The simulated voltage and current waveforms matches well with the experimentally measured current and voltage waveforms and are shown in Fig. T.1.5.

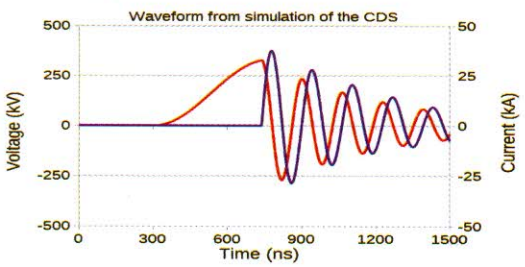

Fig. T.1.5: Simulated voltage and current of the discharge setup

Both, the voltage and the current waveforms, have under-damped oscillations due to the nature of the discharge circuit.

In order to automate the operation of such a system, a two tier control strategy has been followed. The power conditioning of pulsed sources and their control are handled from a micro-controller based system and user commands are handled by a LabVIEW based control program in a personal computer. The complete interfacing of the system is illustrated in the Fig. T.1.6.

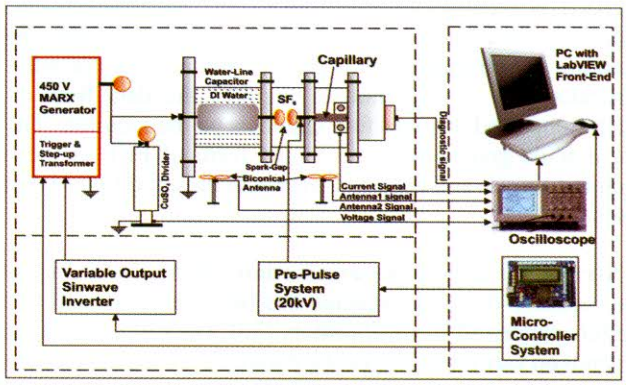

Fig. T.1.6: PC based control and data acquisition system

The power conditioning system consists of a variable output sine-wave inverter and a pre-ionization supply circuitry. The sine-wave inverter can supply 0 to 200 volts, 1 ampere sine-wave output at 50 Hz to a HV transformer having 230 V: 19 kV transformation ratio. The variable output sine-wave inverter topology is based on a controlled rectifier and PWM inverter as shown in Fig.T.1.7. The controlled rectifier utilizes phase-controlled semi converter configuration and the inverter had a sinusoidal pulse width modulated MOSFET full bridge circuitry with an LC filter.

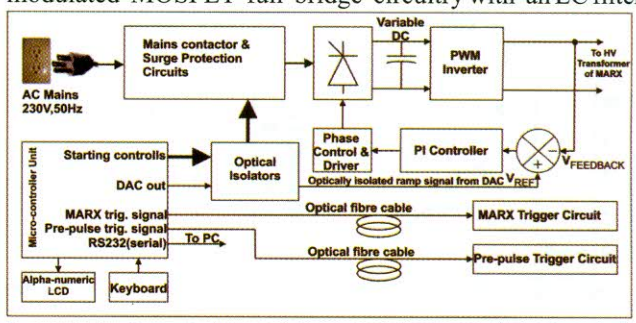

Fig. T.1.7: Interfacing of the micro-controller based control of the power conditioning system

AC sine-wave output from PWM inverter is rectified and fed back to the feedback control circuitry. The feedback control action is governed by a PI controller. The control signal determines the DC output of the controlled rectifier and is generated by comparing the feedback signal with the set reference signal of the micro-controller. The reference analogue signal is generated by the micro-controller through

its DAC output and is optically isolated by an isolation amplifier to avoid unwanted interferences. The DAC provides the ramp signal for limiting the sudden appearance of high voltage across the capacitor charging circuitry associated with the Marx generator. Pre-ionization supply consists of a parallel loaded resonant converter based 20 kV SMPS DC supply and a pulse power circuit.

A graphical user interface (GUI) based window program consisting of three modules has been developed in LABVIEW to collect the data from all the measuring devices, display it, and analyze it. The first module initiates the charging and triggering of the Marx bank and the pre-pulse generator. The second module acquires the data from an oscilloscope and displays four channels on the monitor. The last module generates report in the form of FFT of these acquired signals and then informs about the condition of that discharge.

5. X-ray laser pulse characterization : Soft x-ray lasing by fast capillary discharge scheme has been demonstrated and well characterized in our laboratory [30]. The soft x-ray lasing depends on various experimental parameters which need to be optimized in order to get suitable lasing conditions. These parameters include : discharge current amplitude, its rate of rise, initial gas pressure, pre-pulse conditions (i.e. the pre-pulse amplitude and its timing with respect to the discharge current), and the capillary dimensions (length and inner diameter). A ceramic capillary of 2.8 mm diameter and 15 cm length was used. The various parameters were optimized in order to achieve lasing. Most optimum conditions were found as : discharge current of 40 kA with rise time of 50-60 ns, Ar gas pressure of 0.35 mbar, and a pre-pulse current of ~20 A, passing 5 μs before the main current pulse. A typical optimized signal recorded on the vacuum diode is shown in Fig. T.1.8. One can clearly see a distinct fast x-ray peak of

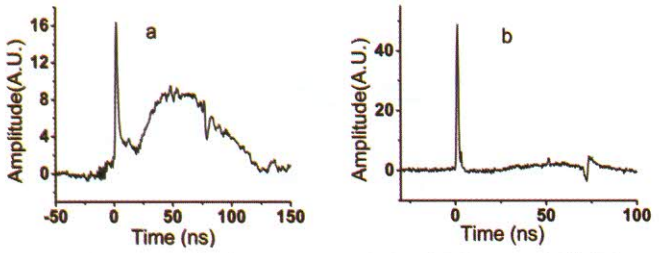

Fig. T.1.8: Vacuum diode signal recorded at (a) 83 cm and (b) 170 cm from the capillary.

~ 1.2 nsFWHM, superimposed over the long duration bremsstrahlung radiation from the plasma. This peak was found to be very sensitive to pre-pulse and completely disappeared in the absence of pre-pulse. When the diode was moved away from the capillary from 83 cm (Fig. T.1.8 a) to 170 cm (Fig.T.1.8 b), it was observed that the background radiation from plasma was selectively reduced compared to the fast x-ray peak observed. This showed that the fast peak has smaller divergence compared to the background. The divergence of the laser beam was measured to be ~ 3.5 mrad by recording the beam profile on a micro-channel plate (MCP) detector placed at different distances from the capillary. The time-integrated spatial profile as recorded on MCP at a large distance ~ 170 cm from the capillary end, is shown in Fig.T.1.9, which clearly shows the distinct laser beam superimposed over a highly divergent background due to the

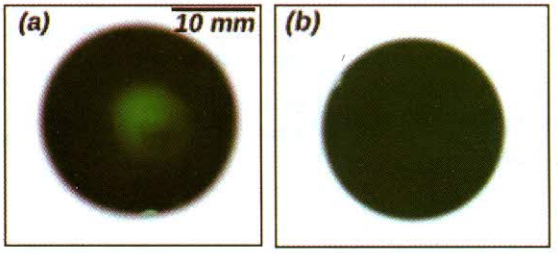

Fig. T.1.9: Spatial profile as recorded on MCP (a) in the presence and (b) in absence of the pre-pulse

bremsstrahlung emission. The wavelength of this laser beam was ascertained by recording its spectrum with a transmission grating (700 lines/mm) and a MCP detector. The time-integrated spectrum with and without pre-pulse is shown in Fig. T.1.10 a and T.1.10 b. Intense monochromatic lasing line emission at 46.9 nm was observed in the spectrum along with its higher diffraction orders. The actual image of the spectrum is shown on the top of the image whereas the intensity plot of the spectrum is displayed below that.

To measure the spatial coherence of this soft x-ray laser, double slit interference experiments were also conducted. Here, a double slit (two 30 μm wide slits separated by 120 μm) was placed in the path of the x-ray laser beam and the resulting interference fringe pattern was recorded on the MCP detector with a very good contrast. The recorded fringe pattern and their intensity plot is shown in Fig. T.1.11. From the interference fringe pattern, the maximum and minimum intensity was measured and then the visibility was calculated to be 85%. For a Gaussian beam, the fringe visibility 'V' can be expressed in terms of the slit separation 'd' and the spatial coherence radius 'L_c' as $V=\exp[-d^2/2L_c^2]$. Using this relation between the visibility and the slit separation, the transverse spatial coherence length was estimated to be ~ 225 μm at a distance of 88 cm from the capillary, where the double slit was placed. In all the above measurements, it was very essential to locate the axis of the x-ray laser beam precisely in space. A quadrant vacuum diode was fabricated in-house for this purpose and it was found to be very useful.

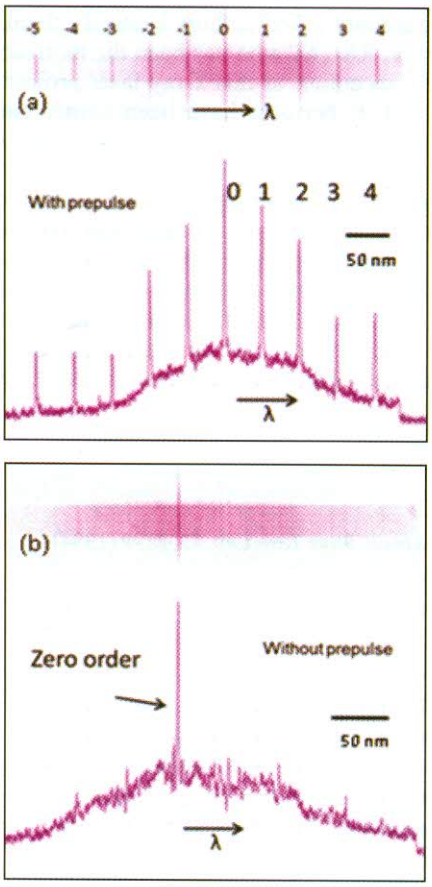

Fig. T.1.10: Spectrum as recorded on MCP in the presence (a) and absence (b) of pre-pulse

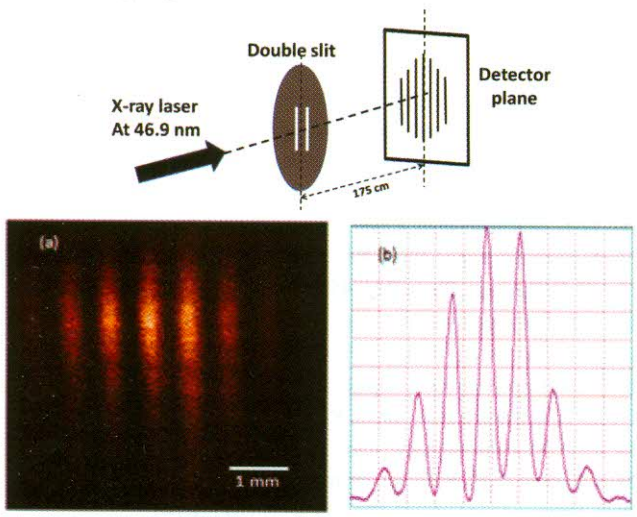

Fig. T.1.11: A schematic diagram for coherence measurement. a) Recorded interference fringe pattern and b) its intensity profile in a direction normal to the fringes

It had a cathode disk made of Cu of 30 mm diameter. The disk was divided into 4 quadrants which were isolated from each other to record the signal separately. Each quadrant of the diode provided the temporal profile of the signal as obtained with single vacuum diode (Fig. T.1.12). From the relative amplitudes of the four signals recorded by the four quadrants, we could easily find out the position of the beam with respect to the diode. This was successfully used to locate the beam axis and align the detectors and other components with respect to beam axis precisely.

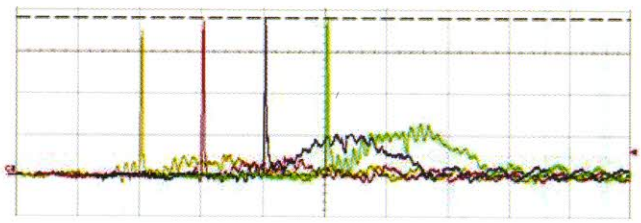

Fig.T.1.12 : Laser peaks recorded in the quadrant vacuum diode in the aligned condition

In order to use this x-ray laser beam in any application, it is important to know its energy content per pulse. The energy measurement required calibration of the in-house developed vacuum diode. This calibration was done with reference to a commercial x-ray diode (AXUV : IRD Inc.). A 1.5 μm Al filter was used to prevent the diode from going into saturation. Comparing the area under the recorded lasing pulse from both the diodes, the quantum efficiency of the vacuum diode was calculated to be 0.104 at 46.9 nm. From this, the energy in single 46.9 nm x-ray laser pulse was calculated to be ~ 2 μJ for a discharge current of 25 kA and argon gas pressure of 0.35 mbar in the 15 cm long capillary. Here, the x-ray laser pulse was recorded on the diodes at a large distance ~ 2.0 m from the source where the contribution of highly divergent bremsstrahlung radiation from plasma is almost negligible compared to the laser pulse in the diode signal. On the driver side, the system was further improved to enhance dI/dt from 7.1×10^{11} A/s to 1.4×10^{12} A/s and as a result, the energy in the laser pulse was also enhanced to 4.0 μJ for a discharge current of 44 kA at initial argon gas pressure of 0.55 mbar in the same ceramic capillary.

The gain-coefficient measurement is also an important parameter of any laser. Therefore, experiments were conducted to study the effect of variation of the plasma column length on the energy of the soft x-ray laser pulse. A ceramic capillary of longer length (~30 cm) was used in this experiment. Firstly, lasing conditions were optimized at the discharge current of ~ 40 kA with quarter period ~ 75 ns, leading to dI/dt ~ 7×10^{11} A/s. The laser pulse energy was obtained to be ~ 2.5 μJ at this optimized conditions. By changing the length of the metallic rods inside the capillary,

the plasma column length was successively reduced to 24 cm, 19 cm, 12 cm and 9 cm. The laser energy was measured at each length of the argon plasma column. The results showed an exponential increase in the laser gain for plasma length below ~15 cm, beyond which the gain increased linearly with

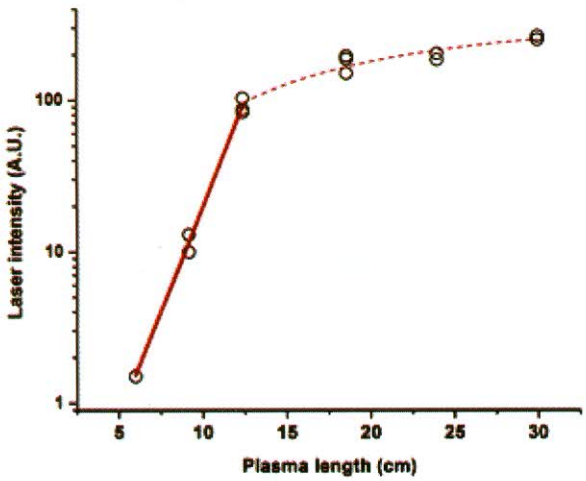

Fig.T.1.13: Experimental curve of laser intensity vs plasma length for measurement of gain-coefficient

length, as shown in Fig. T.1.13. The gain coefficient of this laser was estimated to be ~0.7 cm^{-1} by fitting the exponential part of the curve. Also, this corresponds to a gain-length product of 10.5 for a plasma column length of 15 cm.

6. Conclusion : A compact soft-x-ray laser operating at a wavelength of 46.9 nm has been developed at RRCAT. This x-ray laser is based on electron collisional excitation pumping in highly ionized argon z-pinch plasma driven by fast capillary discharge scheme. The lasing action at 46.9 nm was achieved in highly optimized conditions of various experimental parameters like discharge current amplitude, its rise-time, initial gas pressure in the capillary, pre-pulse amplitude and its onset time with respect to the main pulse etc. This soft x-ray laser was characterized by the measurement of its various parameters like laser pulse duration, divergence, wavelength, spatial coherence, energy per pulse, gain-coefficient etc. Some very useful diagnostics like vacuum diode, quadrant vacuum diode etc. have also been developed for this purpose. Typical measured values of some important laser parameters of this laser (for a plasma column length of 15 cm) are : a) laser pulse duration ~ 1.2 ns, b) divergence ~ 3.5 mrad, c) spatial coherence ~ 224 μm, d) energy per pulse ~ 4.0 μJ, and e) gain-coefficient ~ 0.7 cm^{-1}.

Acknowledgements : The authors sincerely thank Dr P.D. Gupta, Director, RRCAT who has been the motivating force right from the inception of this x-ray laser project. Dr P.A. Naik and Shri C.P. Navathe have been jointly guiding the capillary x-ray laser team and have helped to overcome obstacles from time to time. We would also like to acknowledge the active participation of Dr J.A. Chakera in the initial stages, and Shri K. Aneesh, who has helped the program by his hard work and innovative ideas. The authors would also like to express their thanks to Shri P.K.Tripathi and Shri R.P. Kushwaha in the mechanical fabrication of the capillary discharge system. All the timely help from the laser workshop and the Chemical Treatment Facility is gratefully acknowledged.

References

1. J. J. Rocca *et al.*, Phys. Rev. Lett. 73, 2192 (1994)
2. J. J. Rocca *et al.*, Phys. Rev. Lett. 77, 1476 (1996)
3. S. Heinbuch *et al.*, Optics Express 13, 4050 (2005)
4. A. Ben-Kish, *et al.*, Phys.Rev.Lett.87, 015002 (2001)
5. G. Niimi *et al.*, J. Physics D 34, 2123 (2001)
6. Y. Hayashi *et al.*, Jap. J. Appl. Phys. 47, 977 (2008)
7. N.Sakamoto *et al.*, Jap.J. Appl. Phys. 47, 2250 (2008)
8. Y. Hayashi *et al.*, Jap. J. Appl. Phys. 42, 5285 (2003)
9. Y. Hayashi *et al.*, Jap. J. Appl. Phys. 43, 5564 (2004)
10. G. Tomassetti *et al.*, Euro. Phys. J. D 19, 73 *(2002)*
11. G. Tomassetti *et al.*, Optics Comm. 231, 403 *(2004)*
12. A. Ritucci *et al.*, Phys. Rev. A 70, 023818 (2004)
13. A. Ritucci *et al.*, Appl. Phys. Lett. 86, 101106 (2005)
14. C.A. Tan and K.H. Kwek, J. Phys. D 40, 4787 (2007)
15. C.A.Tan and K.H.Kwek, Phys. Rev. A 75, 043808 (2007)
16. Y. P. Zhao *et al.*, J. Physics D 39, 342 (2006)
17. Y. P. Zhao *et al.*, Appl. Phys. B 99, 535 (2010)
18. Y. Xie, *et al.*, Laser Physics 20, 226 (2010)
19. Y. P. Zhao *et al.*, Optics Letters 36, 3458 (2011)
20. K. Kolacek *et al.*, Physics Report 34, 162 (2008)
21. D. L. Mathews *et al*, Phys. Rev. Lett. 54, 110 (1985)
22. S. Suckewer *et al*, Phys. Rev. Lett. 55, 1753 (1985)
23. W. H. Bennett, Phys. Rev. 45, 890 (1934)
24. V.N. Shlyaptsev *et al.*, Proc. SPIE 2520, 365 (1995)
25. D. E. Kim *et al.*, J. Appl. Phys. 84, 5862 (1998)
26. B. R. Benware *et al.*, Optics Letters 22, 796 (1997)
27. B. R. Benware *et al.*, Phys. Rev. Lett., 81, 5804 (1998)
28. C.D. Macchietto *et al.*, Opt. Lett. 24, 1115 (1999)
29. S. Nigam *et al.*, Rev. Sci. Instrum. 82, 024702 (2011)
30. S. Barnwal *et al.*, Appl. Phys. B, 117, 131 (2014)